Crystal Structure of the 13-cis Isomer of Bacteriorhodopsin in the Dark-adapted State

ARTICLE *in* JOURNAL OF MOLECULAR BIOLOGY · OCTOBER 2005

Impact Factor: 4.33 · DOI: 10.1016/j.jmb.2005.07.021 · Source: PubMed

3 AUTHORS, INCLUDING:

Tsutomu Kouyama
Nagoya University
69 PUBLICATIONS **2,036** CITATIONS

SEE PROFILE

doi:10.1016/j.jmb.2005.07.021 J. Mol. Biol. (2005) 352, 319–328

JMB

Available online at www.sciencedirect.com

SCIENCE DIRECT®

ELSEVIER

Crystal Structure of the 13-*cis* Isomer of Bacteriorhodopsin in the Dark-adapted State

Taichi Nishikawa[1], Midori Murakami[1] and Tsutomu Kouyama[1,2]*

[1]*Department of Physics, Graduate School of Science Nagoya University, Nagoya 464-8602, Japan*

[2]*RIKEN Harima Institute/ SPring-8, 1-1-1, Kouto, Mikazuki, Sayo, Hyogo 679-5148 Japan*

**Corresponding author*

The atomic structure of the *trans* isomer of bacteriorhodopsin was determined previously by using a 3D crystal belonging to the space group *P*622. Here, a structure is reported for another isomer with the 13-*cis*, 15-*syn* retinal in a dark-adapted crystal. Structural comparison of the two isomers indicates that retinal isomerization around the C13=C14 and the C15=N bonds is accompanied by noticeable displacements of a few residues in the vicinity of the retinal Schiff base and small re-arrangement of the hydrogen-bonding network in the proton release channel. On the other hand, aromatic residues surrounding the retinal polyene chain were found to scarcely move during the dark/light adaptation. This result suggests that variation in the structural rigidity within the retinal-binding pocket is one of the important factors ensuring the stereospecific isomerization of retinal.

Keywords: proton pump; retinal; membrane protein; stereo-specificity; isomerization

Introduction

Bacteriorhodopsin (bR), a light-driven proton pump found in the purple membrane of *Halobacterium salinarum*, contains retinal as the chromophore, which is bound *via* a protonated Schiff base linkage to the ε-amino group of Lys216.[1–3] In the dark-adapted (DA) membrane, bacteriorhodopsin takes two conformations that are thermally interconvertible, i.e. one isomer contains all-*trans*, 15-*anti* retinal (bR_{trans}), the other containing 13-*cis*, 15-*syn* retinal (bR_{cis}).[4–7] Each isomer undergoes a distinct photoreaction but, due to an efficient branching reaction from a photoreaction intermediate of the 13-*cis* isomer into the *trans* photocycle, the *trans* isomer becomes the major component in the light-adapted (LA) state.[8–12] A thermal equilibrium between these two isomers is established slowly in the dark and, in the fully dark-adapted state, purple membrane contains a 1:1–1:2 mixture of the *trans* and the 13-*cis* isomer.[4,13] The isomeric composition in the dark-adapted state as well as in the light-adapted state is influenced by several factors, including the medium pH,[14,15] the aggregation state of the protein,[16] the hydration level,[17,18] and the hydraulic pressure.[19–21]

Recent crystallographic studies of the *trans* photoreaction intermediates have revealed that the photo-isomerization of retinal from the all-*trans* to the 13-*cis*, 15-*anti* configuration is followed by a significant up-tilt of the C12–C14 region of retinal that is coupled with large displacements of residues (Leu93 and Trp182) contacting the C13 methyl group of retinal.[22,23] On the other hand, little information has been available as to how much these residues move during the dark adaptation, i.e. during the isomerization of retinal from the all-*trans* to the 13-*cis*, 15-*syn* configuration. By investigating neutron diffraction data at 7 Å resolution from purple membrane, Dencher *et al.* have shown that no large structural change is induced during the dark adaptation.[24] To elucidate a small structural difference between the two isomers, therefore, one needs to accumulate higher-resolution structural data of the 13-*cis* isomer.

We have previously developed the membrane fusion method to prepare a 3D crystal belonging to the space group *P*622.[25] This crystal is composed of stacked membranes, in each of which the trimeric bacteriorhodopsin-lipid complexes are arranged on a honeycomb lattice.[26] It has been shown that bacteriorhodopsin in the *P*622 crystal undergoes the normal dark/light adaptation; i.e. the dark-adapted crystal exhibits an absorption maximum at

Abbreviations used: bR, bacteriorhodopsin; bR_{trans}, the all-*trans* 15-*anti* retinal isomer; bR_{cis}, the 13-*cis*, 15-*syn* retinal isomer; DA, dark-adapted; LA, light-adapted.

E-mail address of the corresponding author: kouyama@bio.phys.nagoya-u.ac.jp

0022-2836/$ - see front matter

560 nm, which shifts to 573 nm upon light adaptation.[27] In this study, the structure of the 13-*cis* isomer contained in the dark-adapted state was determined at 2.5 Å resolution, by comparing diffraction data from a dark-adapted crystal with those from a light-adapted crystal.

Results

Absorption spectra of the all-*trans* and the 13-*cis* isomers

Figure 1 shows absorption changes associated with the primary photoreactions of the *trans* and the 13-*cis* isomers in the *P*622 crystal at 100 K. At this low temperature, a dark-adapted crystal exhibited an absorption peak at 568 nm (spectrum 1), which is noticeably blue-shifted as compared to that of a light-adapted crystal ($\lambda_{max}=576$ nm). As observed for the light-adapted crystal,[28] illumination of the dark-adapted crystal with green light ($\lambda=532$ nm) caused a large red shift of the absorption spectrum (spectrum 2) and, after illumination with red light ($\lambda=678$ nm), the original absorption spectrum was restored. It is noteworthy that the green light-induced absorption change observed for the dark-adapted crystal (spectrum 5) is blue-shifted as compared with that observed for the light-adapted crystal (spectrum 6). This shift can be accounted for by the photoreaction of the 13-*cis* isomer leading to accumulation of a K-like red-shifted product, which is designated K_{cis}.

The difference spectrum associated with the bR_{cis}-to-K_{cis} transition ($\Delta A_{cis}(\lambda)$) could be evaluated by subtracting the contribution of the photoreaction of the *trans* isomer (i.e. the bR_{trans}-to-K_{trans} transition) from spectrum 5. In the actual calculation of $\Delta A_{cis}(\lambda)$, the retinal composition ratio was varied until $\Delta A_{cis}(\lambda)$ had a reasonable profile in the whole wavelength; i.e. $\Delta A_{cis}(\lambda) > 0$ in the long wavelength region. This procedure allowed us to estimate an upper limit of the contribution of bR_{trans} (spectrum 3) to the absorption spectrum of the dark-adapted crystal (spectrum 1). From comparison of these spectra, the content of bR_{cis} in the dark-adapted crystal was estimated to be ~60% or higher. Spectrum 4 shows the absorption spectrum of the 13-*cis* isomer that is calculated when the *trans*:*cis* molar ratio in the dark-adapted crystal is assumed to be ~40:60. This spectrum ($\lambda_{max}=562$ nm) is very similar to that of the apomembrane reconstituted with 13-*cis* retinal and cooled to 80 K,[10] justifying the above assumption about the isomeric composition.

X-radiation-induced absorption changes in a dark-adapted crystal

When a dark-adapted crystal at 100 K was exposed to an X-ray flux of 2×10^{12} photons $mm^{-2}\,s^{-1}$, the absorbance at 568 nm diminished with the increasing exposure time and, instead, the absorption bands at 400–520 nm and at 630–700 nm developed (data not shown). The absorption increase at the long wavelength saturated at an early stage of the X-ray exposure (~2×10^{14} photons mm^{-2}), while the absorption increase at 450 nm lasted for a much longer period (>3×10^{15} photons mm^{-2}). This X-radiation-induced absorption change is different from that observed for a light-adapted crystal,[28] suggesting that modification of the retinal chromophore by X-rays proceeded differently for the all-*trans* and the 13-*cis* isomers.

Structural difference between the two isomers contained in the dark-adapted state

Diffraction data at 2.5 Å resolution from a dark-adapted crystal at 100 K were collected using an X-ray dose of 3×10^{15} photons mm^{-2} per data set (Table 1). This X-ray dose is high enough to cause a significant absorption change. But, no significant peak was detected in a difference electron density map derived from two data sets collected serially from the same crystal. This implies that the X-radiation-induced absorption change accompanies an undetectably small structural change.

The *P*622 crystal was found to shrink slightly during the dark adaptation (i.e. $c=112.3$ Å → 112.0 Å). This

Table 1. Data collection and final refinement statistics

	Light-adapted	Dark-adapted[a]
A. *Data collection*		
Resolution (Å)	46.7–2.3	50.0–2.5
Space group	*P*622	*P*622
Unit cell dimensions		
a (Å)	102.3	102.1
b (Å)	102.3	102.0
c (Å)	112.3	112.0
Data completion (%) (outer shell)	100.0 (99.9)	99.8 (99.6)
Number of unique reflections	15,703	12,446
Multiplicity	9.9	9.2
R_{sym}[b] (%) (outer shell)	4.9 (21.1)	5.6 (50.0)
I/σ (outer shell)	5.9 (1.6)	9.2(1.6)
B. *Refinement*		
Resolution limit (Å)	15.0–2.3	15.0–2.5
Protein residues	228	228
Number of lipid molecules	5	5
Number of water molecules	41	40
Number of ions	0	1
R_{cryst}[c] (%)	24.8	27.1
R_{free} (%)	27.1	30.5
r. m. s. deviation from ideal		
Bond lengths (Å)	0.008	0.009
Bond angles (deg.)	1.16	1.22

[a] Structural refinement of the 13-*cis* isomer was performed after the contribution of the *trans* isomer was subtracted from the diffraction data of the dark-adapted state.

[b] $R_{sym}=\sum_{hkl}\sum_i |I_i-\langle I\rangle|/\sum_{hkl}\sum_i I_i$, where I_i is the intensity of an individual reflection and $\langle I\rangle$ is the mean intensity obtained from multiple observations of symmetry-related reflections.

[c] $R_{cryst}=\Sigma(F_{obs}-|F_{calc}|)/\sum_{hkl}|F_{obs}|$ (5% randomly omitted reflections were used for R_{free}).

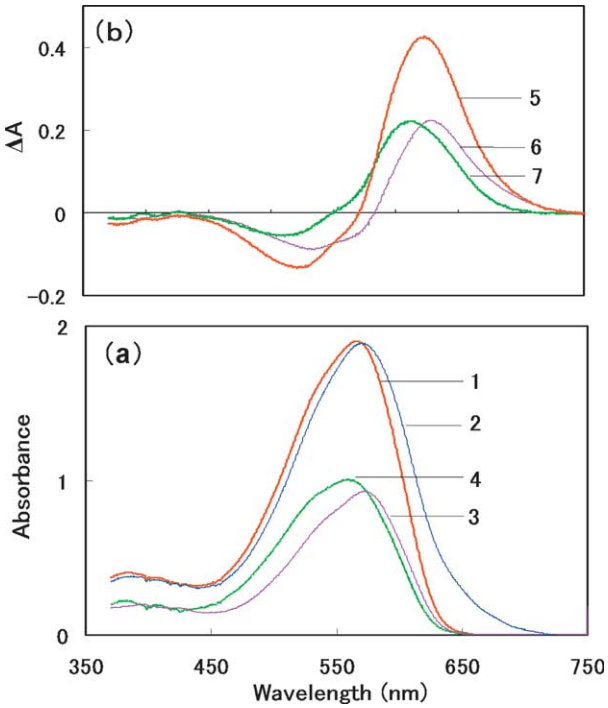

Figure 1. (a) Absorption spectra of dark-adapted and light-adapted crystals at 100 K. Spectra 1 and 2 were recorded after the dark-adapted crystal was illuminated for 1 minute with red light (λ=678 nm; ~1 mW mm^{-2}) and with green light (λ=532 nm; ~0.4 mW mm^{-2}), respectively. Spectrum 3 represents an absorption spectrum of a light-adapted crystal. Spectrum 4 is an absorption spectrum of the 13-*cis* isomer that was derived by subtracting the contribution of the all-*trans* isomer ($\alpha_{trans}\cdot A_{trans}(\lambda)$) from the spectrum of the dark-adapted crystal ($A_{dark}(\lambda)$), i.e.:

$$(1-\alpha_{trans})A_{13\text{–}cis}(\lambda) = (A_{\mathrm{dark}}(\lambda) - \alpha_{trans}A_{trans}(\lambda))$$

where α_{trans} is the content of the all-*trans* isomer in the dark-adapted crystal. The absorption spectrum of the *trans* isomer contained in the dark-adapted state, $A_{trans}(\lambda)$, was assumed to be identical with the absorption spectrum ($A_{\mathrm{light}}(\lambda)$) of a light-adapted crystal at 100 K; i.e.:

$$A_{trans}(\lambda) = \beta A_{\mathrm{light}}(\lambda)$$

where β is a normalization factor. (b) Difference absorption spectra associated with the primary phtotoreactions of the *trans* and the 13-*cis* isomers. Spectrum 5 is the difference spectrum between spectra 1 and 2. The difference spectrum associated with the bR_{cis}-to-K_{cis} transition (spectrum 7), i.e.:

$$\Delta A_{cis}(\lambda) = A_{\mathrm{K}\text{–}cis}(\lambda) - A_{cis}(\lambda))$$

was derived by subtracting the contribution of the primary photoreaction of the *trans* isomer (i.e. $\alpha_{trans}\cdot \Delta A(\lambda)\beta$) from a green-light-induced absorption change (($\Delta A_{\mathrm{dark}}(\lambda)$); spectrum 5 observed for the dark-adapted crystal at 100 K; i.e.:

$$\Delta A_{\mathrm{dark}}(\lambda) = (1-\alpha_{trans})\Delta A_{13\text{–}cis}(\lambda) + \alpha_{trans}\Delta A_{trans}(\lambda)$$

and:

$$\Delta A_{trans}(\lambda) = \beta\Delta A_{\mathrm{light}}(\lambda)$$

where $\Delta A_{\mathrm{light}}(\lambda)$ is a green-light-induced absorption change observed for the light-adapted crystal at 100 K. $\Delta A_{\mathrm{dark}}(\lambda)$ or $\Delta A_{\mathrm{light}}(\lambda)$ was derived by subtracting an absorption spectrum recorded after illumination with red light (λ=678 nm) from that recorded after illumination with green light (λ=532 nm). The parameter $\beta\cdot\alpha_{trans}$ was adjusted until $\alpha_{trans}\cdot\beta\cdot\Delta A_{\mathrm{light}}(\lambda)$ has the same amplitude as $\Delta A_{\mathrm{dark}}(\lambda)$ in the long wavelength region (720–750 nm).

small change of the lattice constant made it difficult to detect directly a structural difference between the two isomers. In fact, an F_0-F_0 difference map derived from the diffraction data of light-adapted and dark-adapted crystals exhibited significant peaks in the solvent region (Figure 2). (It will be shown later that one of these peaks is attributable to binding of sulfate ion near Lys129.) Although positive/negative peaks are seen around the retinal-Lys216 chain (Figure 3(a)), their profiles appeared to be perturbed by the non-isomorphism between the dark-adapted and the light-adapted crystals. To overcome the difficulty in analyzing the F_0-F_0 difference map, we adopted an alternative procedure to determine the structural difference between the two isomers. Namely, the structure of the isomer with the 13-*cis*, 15-*syn* retinal was determined by using the structure factor of the 13-*cis* isomer alone ($F_{\mathrm{DA}\text{-}cis}$), which was evaluated by subtracting the contribution of the *trans* isomer from the diffraction data of a dark-adapted crystal. When the content of the 13-*cis* isomer in the dark-adapted state is large, this procedure can provide more reliable information about the structural change associated with the interconversion between the two isomers (equation (2) in Materials and Methods). During the model building, an F_0-F_0 difference map between the 13-*cis* isomer and the *trans* photocycle L intermediate (Figure 3(b)) was used as an independent guideline for refinement of the 13-*cis*, 15-*syn* configuration of retinal.

In Figures 4 and 5, the structure of the 13-*cis* isomer thus determined is compared with that of the *trans* isomer in the light-adapted state. (The *trans* isomer in the dark-adapted state was not analyzed in the present study.) Comparison of the two isomers indicates that residues (Asp85, Thr89 and Leu93) existing in the vicinity of the retinal Schiff base undergo noticeable displacements during the dark adaptation (Figure 4). On the other hand, residues surrounding the polyene chain of retinal (especially Trp86, Trp182 and Trp189) are left essentially unchanged, irrespective of the up-tilt of the retinal C12–C14 region. It is suggested that the region near the Schiff base is relatively more flexible as compared to the rest of the retinal-binding pocket.

Another structural difference between the two isomers is seen in the conformation of Arg82; i.e. its side-chain directs toward Glu204 in the 13-*cis* isomer, whereas it directs toward Tyr57 in the *trans* isomer (Figure 5). But, as the peptide backbone of Arg82 is immobilized, the guanidinium ion of Arg82 cannot move far enough to make a salt-bridge with Glu194 or Glu204. In both isomers, a water molecule

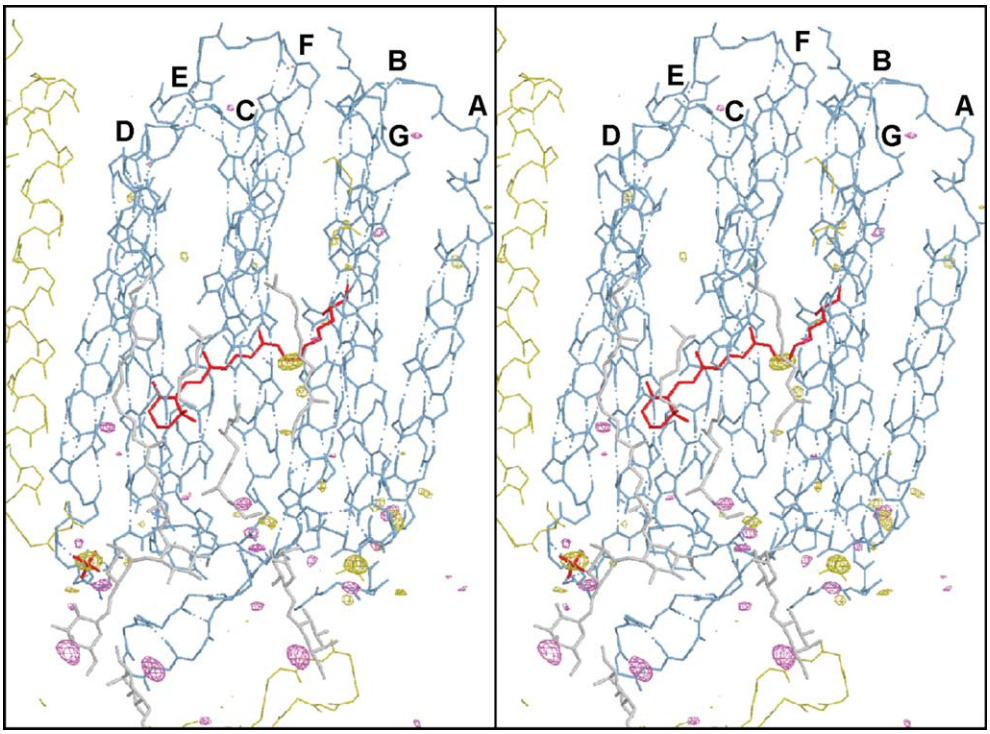

Figure 2. F_0-F_0 difference map ($|F_{DA}|-|F_{LA}|$) between the dark-adapted and the light-adapted states, contoured at 3.6 σ (positive in yellow and negative in purple) and overlaid on the structure model of the 13-*cis* isomer. The retinal-Lys216 chain and a sulfate ion are drawn in red; the glycolipids located in the central part of the trimeric structure are in gray. This Figure and Figures 3, 4, 5 and 7 are drawn with XtalView.[49]

(Wat606) is suggested to mediate interactions between Arg82 and Glu194/Glu204. With respect to water molecules (Wat602, Wat603, Wat604 and Wat605) existing between the Schiff base and Arg82, they undergo small displacements during the light/dark adaptation. Their movements seem to mediate a coupling between the retinal isomerization and the conformational change of Arg82. On the other hand, a water molecule interacting with the indole nitrogen atom of Trp182 (Wat601), which has a high electron density in both the isomers, scarcely moves during the dark adaptation.

In the F_0-F_0 map between the dark-adapted and the light-adapted states (Figure 2), the largest positive peak is seen in the solvent region near Lys129, where a water molecule was placed in the original structural model of the *trans* isomer (PDB id 1iw6). Re-investigation of the $2F_0-F_c$ map of the *trans* isomer suggested the possibility that this site is occupied partially by a sulfate ion that interacts with the amino group of Lys129 (data not shown). In this case, the significant increase in the electron density at this site upon dark adaptation can be accounted for by a higher occupancy of sulfate ion in the dark-adapted state. It should be mentioned that the concentration of precipitant (ammonium sulfate) in the mother solution enveloping a single protein crystal increased inevitably during the dark-adaptation for one day. Thus, it is very likely that the structural change observed in the protein–protein contact region took place in a passive way when anion binding (and presumably cation adsorption) to the protein surface resulted in shrinkage of the crystal along the *c* axis. This interpretation is strengthened by the observation that the head-group of a glycolipid located in the central region of the trimetic structure underwent a significant displacement during the dark adaptation, since this lipid extrudes into the solvent region and interacts with another glycolipid in the adjacent membrane layer (Figure 2).

Discussion

The present result shows that the interconversion between the all-*trans* and the 13-*cis* isomers is accompanied by no significant change in the main-chain structure of the protein interior. The rms deviation for C^{α} positions between the two isomers is 0.19 Å when several residues in flexible regions (Thr5-Pro8, Gly72-Glu74 and Gly231) are not included in the calculation. This result is consistent with previous spectroscopic data, suggesting that the protein tertiary structure as well as the protein-protein interactions (i.e. the exciton interaction of the retinal transition moments) is not altered significantly during the light/dark adaptation.[29] It is consistent also with previous reports concerning the pressure-dependence of the isomeric composition in dark-adapted purple membrane; i.e. it has been shown

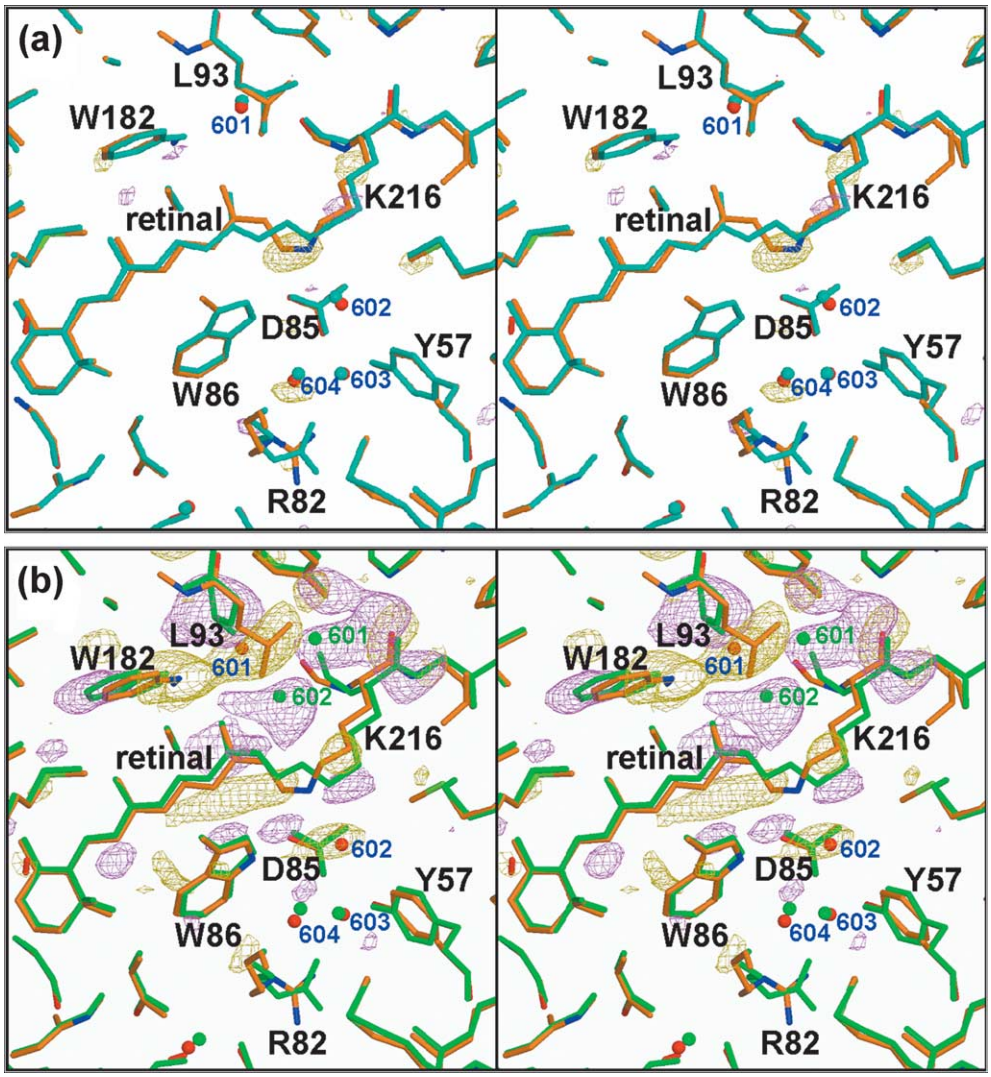

Figure 3. (a) F_0-F_0 difference map ($|F_{DA}|-|F_{LA}|$) between the dark-adapted and the light-adapted states, contoured at 3.2 σ (positive in yellow and negative in purple) and overlaid on the structure models of the 13-*cis* isomer in the dark-adapted state and the *trans* isomer in the light-adapted state. (b) F_0-F_0 difference map ($|F_{DA\text{-}cis}|$-$|F_L|$) between the 13-*cis* isomer and the L intermediate, contoured at 3.2 σ (positive in yellow and negative in purple) and overlaid on their structure models. This map is evaluated by using the previous structural data of the L intermediate.[22] Carbon, nitrogen and oxygen atoms in the 13-*cis* isomer are in gold, blue and red, respectively; atoms in the *trans* isomer and the L intermediates are drawn in cyan and green, respectively.

that a volume difference between the *trans* and the 13-*cis* isomers is very small ($-6\sim-7$ ml mol^{-1}), which is attributable to the formation of a few hydrogen bonds.[19–21]

It has been observed that a significant movement of the polypeptide backbone of Lys216 and the indole ring of Trp182 is induced when the retinal-Lys216 chain in the M intermediate is modified by an X-ray dose of $\sim5\times10^{15}$ photons mm^{-2}.[27] In contrast to the M intermediate, no significant X-radiation-induced structural change was observed in the dark-adapted crystal. This observation may suggest that while the Lys216 side-chain is fully stretched in the M intermediate, it has a relaxed conformation in the dark-adapted state. But it does not exclude the possibility that the retinal itself was modified configurationally during the data collection. In such a situation, it is valuable to compare the present result with previous structural data obtained by NMR. Using an advanced NMR technique, Patzelt *et al.* have observed that the distance between the retinal C14 atom and the indole nitrogen atom of Trp86 increases from 3.6 Å. to 4.4 Å upon the conversion from the all-*trans* to the 13-*cis*, 15-*syn* isomer.[30] When experimental errors are taken into account, the agreement between the X-ray structure and the NMR data is excellent (Table 2). This coincidence suggests that although the retinal chromophore in bR_{cis} might be modified during the data collection, the position of Trp86 does not change greatly. However, the X-ray structure is less compatible with the NMR structure reported by Griffiths *et al.*, who measured the distances between the retinal C14 and the

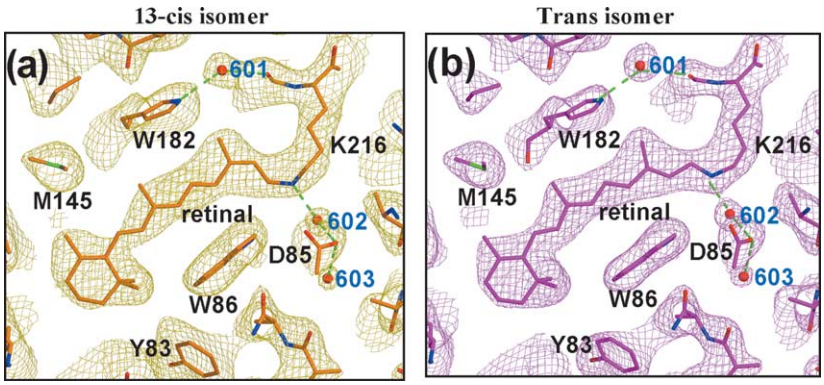

Figure 4. The $2F_o-F_c$ maps of (a) the 13-*cis* isomer in the dark-adapted state and (b) the *trans* isomer in the light-adapted state around the retinal-Lys216 chain, contoured at 1.2 σ and overlaid on their structure models. Carbon atoms in the 13-*cis* isomer and the *trans* isomer are drawn in gold and purple, respectively; nitrogen, oxygen and sulfur atoms are in blue, red and green, respectively.

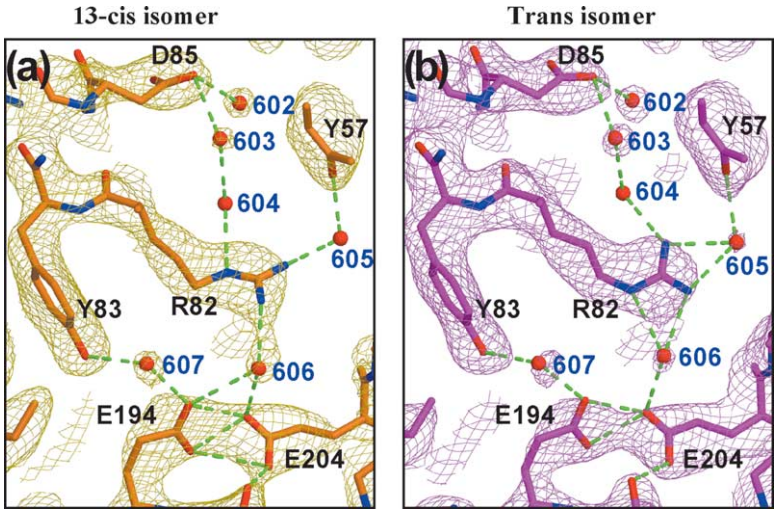

Figure 5. The $2F_o-F_c$ maps of (a) the 13-*cis* isomer in the dark-adapted state and (b) the *trans* isomer in the light-adapted state around Arg82, contoured at 1.4 σ and overlaid on their structure models. Carbon atoms in the 13-*cis* isomer and the *trans* isomer are drawn in gold and purple, respectively; nitrogen and oxygen atoms are in blue and red, respectively.

nearby carboxyl groups (i.e. Asp85 and Asp212).[31] At the present stage, the possibility cannot be excluded that these residues undergo small displacements during the data collection.

Figure 6 shows the most likely conformations of the retinal-binding pocket in bR_{cis} and bR_{trans}. It can be seen that the retinal polyene chain is surrounded by several aromatic residues (Trp86, Trp138, Trp182, Tyr185 and Trp189) and by the peptide backbone of helix F (Pro186). Since these residues are left essentially unchanged during the dark adaptation, the retinal has a limited motional freedom; i.e. the retinal moiety C1–C11 moves only slightly in the longitudinal direction when the retinal isomerization around both the C13=C14 and C15=N double bonds proceeds. On the other

Table 2. Comparison of the X-ray structure with the NMR structure

	bR_{trans}		$bR_{13\text{-}cis}$	
	X-ray	NMR	X-ray	NMR
Retinal-C14 - Trp86-N^{ε}	3.6	3.8[a]	4.4	4.6[a]
Retinal-C14 -Asp85-C^{γ}	5.8	>6.0[b]	6.3	>6.0[b]
Retinal-C14 -Asp212-C^{γ}	4.6	4.4 [b]	4.9	>6.0[b]

All values are in Å.
[a] Patzelt *et al.*[30]
[b] Griffiths *et al.*[31]

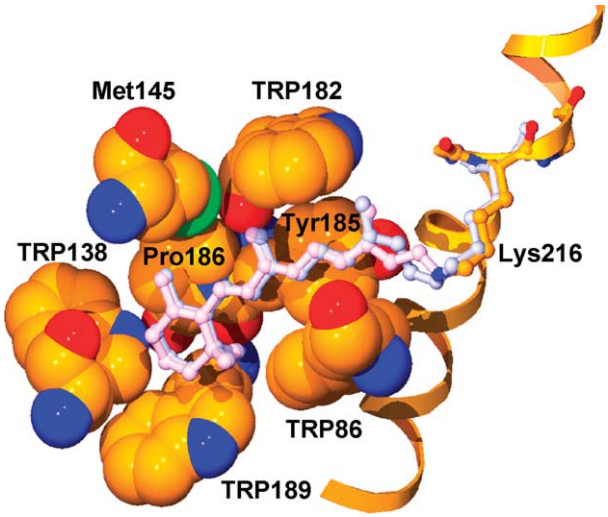

Figure 6. Configuration of the retinal-Lys216 chain in the *trans* isomer (pink tint) and in the 13-*cis* isomer (cyan tint). Aromatic residues surrounding the chromophore are drawn as a CPK model. This Figure is drawn with Swiss PdbViewer.[50]

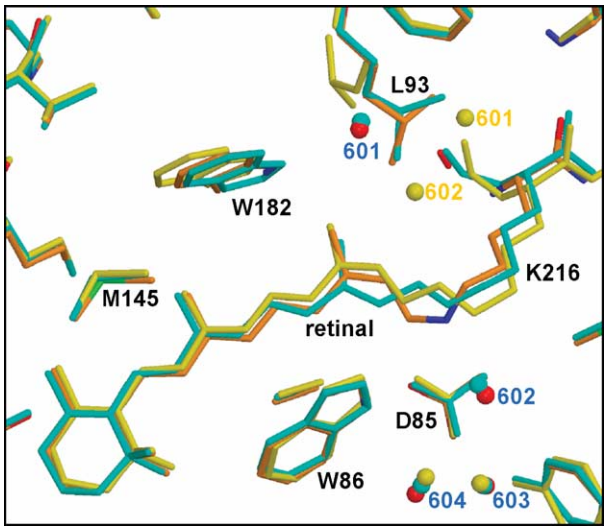

Figure 7. Structural comparison between the 13-*cis* isomer (gold, blue and red), the all-*trans* isomer (cyan) and the L intermediate (yellow).

hand, residues in the vicinity of the retinal Schiff base (Asp85, Thr89 and Leu93) are suggested to be more flexible so that their side-chains undergo noticeable displacements during the dark adaptation. It can be argued that variation in the rigidity within the retinal-binding pocket is one of important factors ensuring the stereospecific isomerization of retinal.

It is noteworthy that most aromatic residues surrounding the polyene chain of retinal are conserved in other archeal rhodopsins.[32–35] Since photo-induced isomerization around the C13=C14 double bond is a crucial event for their functions, it is suggested that these aromatic residues are absolutely required to fix the retinal polyene chain.

In Figure 7, the structure of the 13-*cis* isomer is compared with those of the all-*trans* isomer and the L intermediate. A previous crystallographic study of the L intermediate has indicated that the retinal isomerization around the C13=C14 double bond (i.e. from the all-*trans*, 15-*anti* to the 13-*cis*, 15-*anti* configuration) is accompanied by a pronounced up-tilt of the C12–C14 region that is coupled with a horizontal displacement of Trp182 and a large rotation of the side-chain of Leu93.[22] The latter movements create an open space for a water molecule (Wat602) that is dragged up from the extracellular side of the Schiff base in the K-to-L transition. This vertical movement of water has been suggested to be crucial for the proton pumping activity. On the other hand, there is no indication for large-scale re-distribution of water molecules during the dark/light adaptation; e.g. the water molecule (Wat602) that interacts with the retinal Schiff base moves only slightly.

It has been reported that the pK_a of the purple-to-blue transition is lower for the 13-*cis* isomer than for the *trans* isomer; i.e. the neutral purple form of the 13-*cis* isomer is relatively more stable than that of the *trans* isomer.[36,37] The difference in the thermal stability for the two isomers may be accounted for by a structural difference between the two isomers. Here, it is shown that the guanidinium ion of Arg82 is directed towards Glu204 during the dark adaptation. Our recent crystallographic data of an acid blue form have indicated that the paired structure of Glu194 and Glu204 (i.e. residues comprising the proton release complex) is broken when the purple-to-blue transition is induced by anion binding to the proton-release channel.[38] It is natural to suppose that the re-orientation of the guanidinium ion of Arg82 strengthens the paired structure of Glu194 and Glu204 and thereby makes the neutral purple form of the 13-*cis* isomer more stable as compared to that of the *trans* isomer.

Although a large structural change in the side-chain of Arg82 is also induced upon formation of the M intermediate,[27,39–41] the structural change induced during the dark/light adaptation is essentially different from that induced during the *trans* photocycle. The structural model of the M intermediate generated at room temperature indicates that isomerization of retinal around the double bond (i.e. the C13=C14 bond) is followed by downward movement of the polypeptide backbone of Lys216, which evokes allosteric structural changes in the proton release channel, including a relative sliding motion between helices F and G, disruption of the paired structure of Glu194 and Glu204, formation of a salt-bridge between Arg82 and Glu204, and a horizontal movement of the extracellular half of helix C.[27] It is shown here that isomerization around the C13=C14 and the C15=N double bonds during the dark adaptation is accompanied by a small displacement of the

polypeptide backbone of Lys216. It appears that the relatively smaller structural change observed during the dark adaptation is ultimately attributable to the flexibility of the side-chain of Lys216, by which a confliction between the 13-*cis*, 15-*syn* retinal and its surrounding residues can be absorbed. A similar conclusion has been suggested by a recent crystallographic analysis of *Anabaena* sensory rhodopsin, in which retinal can take either the all-*trans* or the 13-*cis*, 15-*syn* configuration in the dark.[42]

Materials and methods

Protein purification and crystallization

Purple membrane was isolated from *Halobacterium salinarum* JW3 and purified according to the established procedure.[43] Crystals were grown by the membrane fusion method essentially as described,[25] but with slight modifications. Briefly, purple membrane sheets (5 mg ml^{-1}) were vesicularized at 32 °C in the presence of 2.5 mg ml^{-1} of octylthioglucoside, 1.0 M ammonium sulfate, 0.16 M NaCl, 12% (w/v) trehalose, 0.04% (w/v) NaN_3 and 0.08 M sodium citrate (pH 5.2).[44] The resultant vesicular assemblies of bacteriorhodopsin were concentrated at 10 °C by the sitting-drop, vapor-diffusion method using a reservoir solution containing 1.9–2.0 M ammonium sulfate. Incubation for three to six months yielded hexagonal crystals exhibiting birefringence. For dark adaptation, a single crystal captured in a cryo-loop was sealed in a black-painted plastic container. After the crystal was dark-adapted at 288 K for one day, the cryo-loop was separated from the plastic container and then immersed into liquid nitrogen; this operation was done in the dark.

Measurements of absorption spectra and absorption kinetics

For absorption measurements, the frozen crystal was mounted on a goniometer attached to a microscope and placed in a flow of cold nitrogen gas from a cryostreamer (Oxford CC-12). Absorption changes induced by green light (λ=532 nm, 1 mW mm^{-2}) or red light (λ=678 nm; 4 mW mm^{-2}) were measured using a micro-spectrophotometer, in which monochromatic light from a double monochromator (Shimadzu UV350A) was focused on the frozen crystal by a combination of quartz lenses and two diaphragms in a home-made microscope and the measuring light passing through the crystal was focused again on a pinhole attached before a photomultiplier tube.[17] The photocurrent was converted to a voltage signal by a logarithm amplifier (Analog Devices 775P) and then digitalized for data acquisition.

X-radiation-induced absorption changes in a dark-adapted crystal were measured using an on-line micro-spectrophotometer constructed at the beamline SPring8-BL44B2.[45]

Data collection and scaling

X-ray diffraction measurements were performed at the beamlines SPring8-BL40B2 and -BL44B2, where a dark-adapted crystal kept at 100 K was exposed to a monochromatic X-ray beam at wavelength of 1.0 Å with an X-ray flux rate of $\sim 2\times10^{12}$ photons mm^{-2} s^{-1}. Diffraction data were collected using a CCD detector (MarResearch marccd165), with an oscillation range of 1° and an X-ray flux of $\sim 4\times10^{13}$ photons mm^{-2} per image. Indexing and integration of diffraction spots were carried out with Mosflm 6.1.[46] The scaling of data was done using SCALA in the CCP4 program suites.[47]

Structural refinement of the 13-*cis* isomer

Structural analysis of the dark-adapted state was performed with CNS[48] and with XtalView.[49] Firstly, the structural model of the *trans* isomer (PDB id 1iw6) was subjected to a rigid-body refinement and an individual temperature factor refinement. The $2F_o-F_c$ map calculated at this stage suggested that the main-chain structure in the protein interior did not alter significantly during the light/dark adaptation. It was suggested, however, that the crystal shrinkage accompanied noticeable conformational changes in the N-terminal region (Thr5-Pro8) and the BC loop (Gly72-Glu74). This implies that we need to abandon the assumption that the *trans* isomer contained in the dark-adapted state has the same conformation as that found in the light-adapted state. Therefore, the difference between the structure factors for the dark-adapted and the light-adapted states (F_{DA} and F_{LA}, respectively) is given by:

$$F_{DA}-F_{LA} = (F_{DA-cis}-F_{DA-trans})(1-\alpha) + (F_{DA-trans}-F_{LA})\alpha \quad (1)$$

where $F_{DA\text{-}cis}$ and $F_{DA\text{-}trans}$ are the structure factors for the 13-*cis* and the *trans* isomers, respectively, in the dark-adapted state; α is the content of the *trans* isomer in the dark-adapted state. Equation (1) is derived on the assumption that only the *trans* isomer is contained in the light-adapted state (i.e. $F_{LA}=F_{LA\text{-}trans}$, where $F_{LA\text{-}trans}$ is the structure factor of the *trans* isomer in the light-adapted state). But, since no reliable information is available as to how much the structure of the *trans* isomer in the dark adapted state is different from that of the *trans* isomer in the light-adapted state, the second term in the right-hand side (i.e. $F_{DA\text{-}trans}-F_{LA\text{-}trans}$) cannot be neglected. If this term is not small, it would cause a large perturbation in the calculation of the difference amplitude ($|F_{DA\text{-}cis}|-|F_{DA\text{-}trans}|$) from the experimentally available data (i.e. $|F_{DA}|$-$|F_{LA}|$); in the worst case, the sign of the difference amplitude would be reversed. In other words, the $|F_{DA}|$-$|F_{LA}|$ difference map would provide erroneous information about a structural difference between the two isomers, unless the effect of the non-isomorphism is negligible. As a matter of fact, a crystal shrinkage was always induced during the dark adaptation, primarily because of difficulty in controlling the concentration of salt in a mother solution enclosing a single protein crystal for a long period. It was observed occasionally that salt crystals grew during the dark adaptation. Merging diffraction data from dark-adapted crystals having cell dimensions close to those observed for light-adapted crystals was effective for improving the signal-to-noise ratio, but the problem of the non-isomorphism itself was not removed completely. Under such circumstances, we adopted the following procedure for model building of the 13-*cis* isomer. In brief, the structure factor of the 13-*cis* isomer alone was evaluated by subtracting the contribution of the *trans* isomer from the diffraction data of the dark-adapted state:

$$\{F_{DA} - F_{LA}\alpha\}/(1-\alpha)$$
$$= F_{DA-cis} + (F_{DA-trans} - F_{LA})\alpha/(1-\alpha) \quad (2)$$

When α is small, this quantity substantially stands for the structure factor $F_{DA\text{-}cis}$; i.e. the second term in the right-hand side would not perturb the phase information of the first term significantly (i.e. $F_{DA\text{-}cis}$), unless the amplitude $|F_{DA\text{-}cis}|$ is very small. In the actual evaluation of the structure factor $|F_{DA\text{-}cis}|$, the isomeric composition in the dark-adapted state (i.e. a 40:60 mixture of bR_{trans} and bR_{cis}) was taken into account. The structure factor $F_{DA\text{-}cis}$ thus obtained was used in simulated-annealing refinement of the 13-*cis* isomer. The statistics of the final refinement is shown in Table 1.

Requests for materials should be addressed to T.K. (kouyama@bio.phys.nagoya-u.ac.jp).

Protein Data Bank accession codes

Crystallographic coordinates of the light-adapted and the dark-adapted bacteriorhodopsin have been deposited with the RCSB Protein Data Bank with accession codes 1iw6 and 1X0s, respectively.

Acknowledgements

This work was supported by grants-in-aid from the Ministry of Education, Science, and Culture of Japan and partly by the National Project on Protein Structural and Functional Analyses.

References

1. Facciotti, M. T., Rouhani-Manshadi, S. & Glaeser, R. M. (2004). Energy transduction in transmembrane ion pumps. *Trend. Biochem. Sci.* **29**, 445–451.
2. Belrhali, H., Nollert, P., Royant, A., Menzel, C., Rosenbusch, J. P., Landau, E. M. & Pebay-Peyroula, E. (1999). Protein, lipid and water organization in bacteriorhodopsin crystals: a molecular view of the purple membrane at 1.9 Å resolution. *Proteins: Struct. Funct. Genet.* **7**, 909–917.
3. Luecke, H., Schober, B., Richter, H.-T., Cartailler, J.-P. & Lanyi, J. K. (1999). Structure of bacteriorhodopsin at 1.55 Å resolution. *J. Mol. Biol.* **291**, 899–911.
4. Stoeckenius, W., Lozier, R. H. & Bogomolni, R. A. (1979). Bacteriorhodopsin and the purple membrane of halobacteria. *Biochim. Biophys. Acta*, **505**, 215–278.
5. Habison, G. S., Smith, S. O., Pardoen, J. A., Winke, C., Lugtenburg, J., Mathies, R. A. & Griffin, R. G. (1984). Dark-adapted bacteriorhodopsin contains 13-*cis*, 15-*syn* and all-trans, 15-*anti* retinal Schiff base. *Proc. Natl Acad. Sci. USA*, **81**, 1706–1709.
6. Smith, S. O., Pardoen, J. A., Lugtenburg, J. & Mathies, R. A. (1987). Vibrational analysis of the 13-*cis*-retinal chromophore in dark-adapted bacteriorhodopsin. *J. Phys. Chem.* **91**, 804–819.
7. Smith, S. O., de Groot, H. J. M., Gebhard, R., Courtin, J. M. L., Lugtenburg, J., Herzfeld, J. & Griffin, R. G. (1989). Structure and protein environment of the retinal chromophore in light- and dark-adapted bacteriorhodopsin studied by solid-state NMR. *Biochemistry*, **28**, 8897–8904.
8. Sperling, W., Carl, P., Patferty, Ch. N. & Dencher, N. A. (1977). Photochemistry and dark equilibrium of retinal isomers and bacteriorhodopsin isomers. *Biophys. Struct. Mech.* **3**, 79–94.
9. Lozier, R. H., Niederberger, W., Ottolenghi, M., Sivorinovsky, G. & Stoeckenius, W. (1978). On the photocycles of light- and dark-adapted bacteriorhodopsin. In *Energetics and Structure of Halophilic Microorganisms* (Caplan, S. R. & Ginzburg, M., eds), pp. 123–139, Elsevier, North-Holland Biomedical Press.
10. Iwasa, T., Tokunaga, F. & Yoshizawa, T. (1981). Photochemical reaction of 13-*cis* bacteriorhodpsin studied by low temperature spectrophotometry. *Photochem. Photobiol.* **33**, 539–545.
11. Hofrichter, J., Henry, E. R. & Lozier, R. H. (1989). Photocycles of baceriorhodopsin in light-adapted and dark-adapted purple membrane studied by time-resoluved absorption spectroscopy. *Biophys. J.* **56**, 693–706.
12. Gergely, C., Ganea, C. & Varo, G. (1994). Combined optical and photoelectric study of the photocycle of 13-*cis* bacteriorhodopsin. *Biophys. J.* **67**, 855–861.
13. Scherrer, P., Mathew, M. K., Sperling, W. & Stoeckenius, W. (1989). Retinal isomer ratio in dark-adapted purple membrane and bacteriorhodopsin monomers. *Biochemistry*, **28**, 829–834.
14. Mowery, P. C., Lozier, R. H., Chae, Q., Tseng, Y. W., Taylor, M. & Stoeckenius, W. (1979). Effect of acid pH on the absorption spectra and photoreactions of bacteriorhodopsin. *Biochemistry*, **18**, 4100–4107.
15. de Groot, H. J., Smith, S. O., Courtin, J., van den Berg, E., Winkel, C., Lugtenburg, J. *et al*. (1990). Solid-state ^{13}C and ^{15}N NMR study of the low pH forms of bacteriorhodopsin. *Biochemistry*, **29**, 6873–6883.
16. Dencher, N. A., Kohl, K.-D. & Heyn, M. P (1983). Photochemical cycle and light-dark adaptation of monomeric and aggregated bacteriorhodopsin in vari ous lipid environments. *Biochemistry*, **22**, 1323–1334.
17. Kouyama, T., Bogomolni, R. & Stoeckenius, W. (1985). Photoconversion from the light-adapted to the dark-adapted state of bacteriorhodopsin. *Biophys. J.* **48**, 201–208.
18. Brown, L. S. & Chamorovsky, S. K. (1993). Light adaptation blockage in dehydrated purple membrane does not result from retinal isomerization inhibition. *J. Photochem. Photobiol. B*, **18**, 123–126.
19. Tsuda, M. & Ebrey, T. G. (1980). Effect of high pressure on the absorption spectrum and isomeric composition of bacteriorhodopsin. *Biophys. J.* **30**, 149–157.
20. Schulte, A. & Bradley, L. I. (1995). High-pressure near-infrared Raman spectroscopy of bacteriorhodopsin light to dark adaptation. *Biophys. J.* **69**, 1554–1562.
21. Bryl, K. & Yoshihara, K. (2002). Two processes lead to a stable all-*trans* and 13-*cis* isomer equilibrium in dark-adapted bacteriorhodopsin: Effect of high presuure on bacteriorhodopsin, bacteriorhodopsin mutant D96N and fluuoro-bacteriorhodopsin analogues. *Eur. Biophys. J.* **31**, 539–548.
22. Kouyama, T., Nishikawa, T., Tokuhisa, T. & Okumura, H. (2004). Crystal structure of the L intermediate of bacteriorhodopsin: evidence for vertical translocation of a water molecule during the proton pumping cycle. *J. Mol. Biol.* **335**, 531–546.
23. Royant, A., Edman, K., Ursby, T., Pebay-Peyroula, E., Landau, E. M. & Neutze, R. (2000). Helix deformation is coupled to vectorial proton transport in the photocycle of bacteriorhodopsin. *Nature*, **406**, 645–648.

24. Dencher, N. A., Papadopoulos, G., Dresselhaus, D. & Bueldt, G. (1990). Light and dark-adapted bacteriorhodopsin: a time-resolved neutron diffraction study. *Biochim. Biophys. Acta*, **1026**, 51–56.
25. Takeda, K., Sato, H., Hino, T., Kono, M., Fukuda, K., Sakurai, I. *et al*. (1998). A novel three-dimensional crystal of bacteriorhodopsin obtained by successive fusion of the vesicular assemblies. *J. Mol. Biol.* **283**, 463–474.
26. Sato, H., Takeda, K., Tani, K., Hino, T., Okada, T., Nakasako, M. *et al*. (1999). Specific lipid-protein interactions in a novel honeycomb lattice structure of bacteriorhodopsin. *Acta Crystallog. sect. D*, **55**, 1251–1256.
27. Takeda, K., Matsui, Y., Kamiya, N., Adachi, S., Okumura, H. & Kouyama, T. (2004). Crystal structure of the M intermediate of bacteriorhodopsin: allosteric structural changes mediated by sliding movement of a transmembrane helix. *J. Mol. Biol.* **341**, 1023–1037.
28. Matsui, Y., Sakai, K., Murakami, M., Shiro, Y., Adachi, S., Okumura, H. & Kouyama, T. (2002). Specific damages induced by X-ray radiation and structural changes in the primary photoreaction of bacteriorhodopsin. *J. Mol. Biol.* **324**, 469–481.
29. Becher, B. & Cassim, J. Y. (1976). Effects of light adaptation on the purple membrane structure of *Halobacterium halobium*. *Biophys. J.* **16**, 1183–1200.
30. Patzelt, H., Simon, B., terLaak, A., Kessler, B., Kuhne, R., Schmieder, P. *et al*. (2002). The structures of the active center in dark-adapted bacteriorhodopsin by solution-state NMR spectroscopy. *Proc. Natl Acad. Sci. USA*, **99**, 9765–9770.
31. Griffiths, J. M., Bennett, A. E., Engelhard, M., Siebert, F., Raap, J., Lugtenburg, J. *et al*. (2000). Structural investigation of the active site in bacteriorhodopsin: geometric constraints on the roles of Asp-85 and Asp-212 in the proton-pumping mechanism from solid state NMR. *Biochemistry*, **39**, 362–371.
32. Enami, N., Okumura, H. & Kouyama, T. (2002). X-ray crystallographic study of archaerhodopsin. *J. Photosci.* **9**, 320–322.
33. Royant, A., Nollert, P., Edmani, K., Neutze, R., Landau, E. M., Pebay-Peyroula, E. & Navarro, J. (2001). X-ray structure of sensory rhodopsin II at 2.1-Å resolution. *Proc. Natl Acad. Sci. USA*, **98**, 10131–10136.
34. Luecke, H., Schobert, B., Lanyi, J. K., Spudich, E. N. & Spudich, J. L. (2001). Crystal structure of sensory rhodopsin II at 2.4 Å: insights into color tuning and transducer interaction. *Science*, **293**, 1499–1503.
35. Kolbe, M., Besir, H., Essen, L. O. & Oesterhelt, D. (2000). Structure of the light-driven chloride pump halorhodopsin at 1.8 Å resolution. *Science*, **288**, 1390–1396.
36. Chen, D.-L., Wang, G.-Y., Xu, B. & Hu, K.-S. (2002). All-*trans* to 13-*cis* retinal isomerization in light-adapted bacteriorhodopsin at acidic pH. *J. Photochem. Photobiol. B*, **66**, 188–194.
37. Balashov, S. P., Imasheva, E. S., Govindjee, R., Sheves, M. & Ebrey, T. G. (1996). Evidence that asparatate-85 has a higher pK_a in all-trans than in 13-*cis* bacteriorhodopsin. *Biophys. J.* **71**, 1973–1984.
38. Okumura, H., Murakami, M. & Kouyama, T. (2005). Crystal structures of acid blue and alkaline purple forms of bacteriorhodopsin. *J. Mol. Biol.* **351**, 481–495.
39. Luecke, H., Schobert, B., Richter, H. T., Cartailler, J.-P. & Lanyi, J. K. (1999). Structural changes in bacteriorhodopsin during ion transport at 2 Å resolution. *Science*, **286**, 255–260.
40. Sass, H. J., Buldt, G., Gessenich, R., Hehn, D., Neff, D., Schlesinger, R. *et al*. (2000). Structural alterations for proton translocation in the M state of wild-type bacteriorhodopsin. *Nature*, **406**, 649–653.
41. Facciotti, M. T., Rouhani, S., Burkard, F. T., Betancourt, F. M., Downing, K. H., Rose, R. B. *et al*. (2001). Structure of an early intermediate in the M-state phase of the bacteriorhodopsin photocycle. *Biophys. J.* **81**, 3442–3455.
42. Vogeley, L., Sineshchekov, O. A., Trivedi, V. D., Sasaki, J., Spudich, J. L. & Luecke, H. (2005). *Anabaena* sensory rhodopsin: a photochromic color sensor at 2.0 Å. *Science*, **306**, 1390–1393.
43. Oesterhelt, D. & Stoeckenius, W. (1974). Isolation of the cell membrane of *Halobacterium halobium* and its fractionation into red and purple membrane. *Methods Enzymol.* **31**, 667–678.
44. Kouyama, T., Yamamoto, M., Kamiya, N., Iwasaki, H., Ueki, T. & Sakurai, I. (1994). Polyhedral assembly of a membrane protein in its three-dimensional crystal. *J. Mol. Biol.* **236**, 990–994.
45. Sakai, K., Matsui, Y., Kouyama, T., Shiro, Y. & Adachi, S. (2002). Optical monitoring of freeze-trapped reaction intermediates in protein crystals: a microspectrophotometer for cryogenic protein crystallography. *J. Appl. Crystallog. sect. D*, **35**, 270–273.
46. Steller, I., Bolotovsky, B. & Rossmann, M. G. (1997). An algorithm for automatic indexing of oscillation images using Fourier analysis. *J. Appl. Crystallog. sect. D*, **30**, 1036–1040.
47. Collaborative Computating Project Number 4. (1994). The CCP4 suite: programs for protein crystallography. *Acta Crystallog. sect. D*, **50**, 760–763.
48. Brünger, A. T., Adams, P. D., Glore, G. M., Delano, W. L., Gros, P., Grosse-Kunstleve, R. W. *et al*. (1998). Crystallography and NMR system (CNS.): a new software system for macromolecular structure determination. *Acta Crystallog. sect. D*, **54**, 905–921.
49. McRee, D. E. (1993). *Practical Protein Crystallography*, Academic Press, San Diego.
50. Guex, N. & Peitsch, M. C. (1997). SWISS-MODEL and the Swiss-PdbViewer: an environment for comparative protein modeling. *Electrophoresis*, **18**, 14–23.

Edited by R. Huber

(Received 31 March 2005; received in revised form 4 July 2005; accepted 7 July 2005)
Available online 26 July 2005